

RESEARCH ARTICLE



Design, synthesis and evaluation of novel cinnamic acid derivatives bearing *N*-benzyl pyridinium moiety as multifunctional cholinesterase inhibitors for Alzheimer's disease

Jin-Shuai Lan^{a*}, Jian-Wei Hou^{a*}, Yun Liu^a, Yue Ding^a, Yong Zhang^a, Ling Li^a and Tong Zhang^b

^aExperiment Center of Teaching & Learning, Shanghai University of Traditional Chinese Medicine, Shanghai, China; ^bSchool of Pharmacy, Shanghai University of Traditional Chinese Medicine, Shanghai, China

ABSTRACT

A novel family of cinnamic acid derivatives has been developed to be multifunctional cholinesterase inhibitors against AD by fusing *N*-benzyl pyridinium moiety and different substituted cinnamic acids. *In vitro* studies showed that most compounds were endowed with a noteworthy ability to inhibit cholinesterase, self-induced A β (1–42) aggregation, and to chelate metal ions. Especially, compound **5I** showed potent cholinesterase inhibitory activity (IC₅₀, 12.1 nM for *ee*AChE, 8.6 nM for *h*AChE, 2.6 μ M for *eq*BuChE and 4.4 μ M for *h*BuChE) and the highest selectivity toward AChE over BuChE. It also showed good inhibition of A β (1–42) aggregation (64.7% at 20 μ M) and good neuroprotection on PC12 cells against amyloid-induced cell toxicity. Finally, compound **5I** could penetrate the BBB, as forecasted by the PAMPA-BBB assay and proved in OF1 mice by *ex vivo* experiments. Overall, compound **5I** seems to be a promising lead compound for the treatment of Alzheimer's diseases.

ARTICLE HISTORY

Received 26 July 2016
Revised 10 October 2016
Accepted 17 October 2016

KEYWORDS

Alzheimer's disease;
 β -amyloid aggregation;
benzylpyridinium; cinnamic acid; metal chelator;
neuroprotection

Introduction


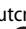


Alzheimer's disease (AD) is a fatal neurodegenerative disorder that is clinically associated with cognitive impairment, language skill loss and dementia¹. To date almost 48 million elderly people are affected by AD, and this number is estimated to show unparalleled growth and increase to spread 131.5 million by 2050². Although the etiopathogenesis of AD is unclear, multiple factors such as amyloid- β (A β) deposits, low levels of acetylcholine (ACh), τ -protein aggregation, dyshomeostasis of biometals and oxidative stress, play a vital role in the pathogenesis of AD³. The current therapeutic options against AD are composed by one *N*-methyl-D-aspartate (NMDA) receptor antagonist and three acetylcholinesterase (AChE) inhibitors, namely memantine (NMDA), donepezil, rivastigmine and galantamine (AChE)⁴. Nevertheless, these marketed drugs modestly alleviate the symptoms but cannot cure brain damage or stop neuronal degeneration.

AChE and BuChE play a role in cholinergic signaling. According to the cholinergic hypothesis, the decrease in ACh levels results in memory loss and cognitive impairment, and the clinical restoration of cholinergic function is believed to alleviate AD symptoms^{5,6}. Furthermore, studies have illustrated that AChE interacts with A β through the peripheral anionic site (PAS) promoting the formation of steady AChE-A β complexes, which are more toxic than single A β peptides⁷. Therefore, dual-site AChE inhibitors may be promising AD drug candidates^{8,9}.

Among multiple factors, neurotoxic A β plaques in the brain are a key contributing factor in the pathology of AD. A β (1–40) and A β (1–42) are the key isoforms of A β peptides. A β (1–42) may aggregate more rapidly and show stronger neuron cytotoxicity

than A β (1–40) does^{10,11}. Preventing the formation and accumulation of A β is a probable therapeutic strategy for AD. The dyshomeostasis of metal ions such as Cu, Fe and Zn is commonly observed in many critical aspects of AD¹². The Cu²⁺ present in the brain at an abnormally high concentration interacts with A β , leading to the accelerated formation of neurofibrillary tangles (NFTs) and generate reactive oxygen species (ROS), which further induce oxidative impairment in the brain¹³. Moreover, abnormally high levels of redox-active metal ions, such as Fe²⁺ and Cu²⁺, in the brain may lead to the formation of ROS¹⁴. Notably, compared with the normal levels of metal ions in brain, the subtraction of physiologically essential metals may lead to risk. Consequently, reducing the abnormally high concentration of metals in the brain by chelating the metals is an additional logical approach for AD treatment. Oxidative stress also plays a crucial role in the development of neurodegenerative disorders such as AD. It has been hypothesised that the antioxidant defence system cannot neutralize oxidative species in elderly people¹⁵. The oxidative stress theory of ageing also suggests that oxidative damage plays an important role in neuronal degeneration¹⁶. Therefore, drugs that can scavenge oxygen radicals may be used to prevent AD.

Due to the pathological complication of AD, the multi-target-directed ligand (MTDL) design strategy has been proposed, and a range of compounds have been developed to act on various targets^{17–21}. In AD, the effectiveness of multifunctional molecules with two or more distinct pharmacological properties being properly incorporated is higher than that of single-targeted drugs²².

CONTACT Tong Zhang  zhangtongshutcm@hotmail.com  School of Pharmacy, Shanghai University of Traditional Chinese Medicine, Shanghai 201203, China; Yue Ding  dingyue-2001@hotmail.com  Experiment Center of Teaching & Learning, Shanghai University of Traditional Chinese Medicine, Shanghai 201203, China.

*These authors contributed equally to this work.

© 2017 The Author(s). Published by Informa UK Limited, trading as Taylor & Francis Group

This is an Open Access article distributed under the terms of the Creative Commons Attribution License (<http://creativecommons.org/licenses/by/4.0/>), which permits unrestricted use, distribution, and reproduction in any medium, provided the original work is properly cited.

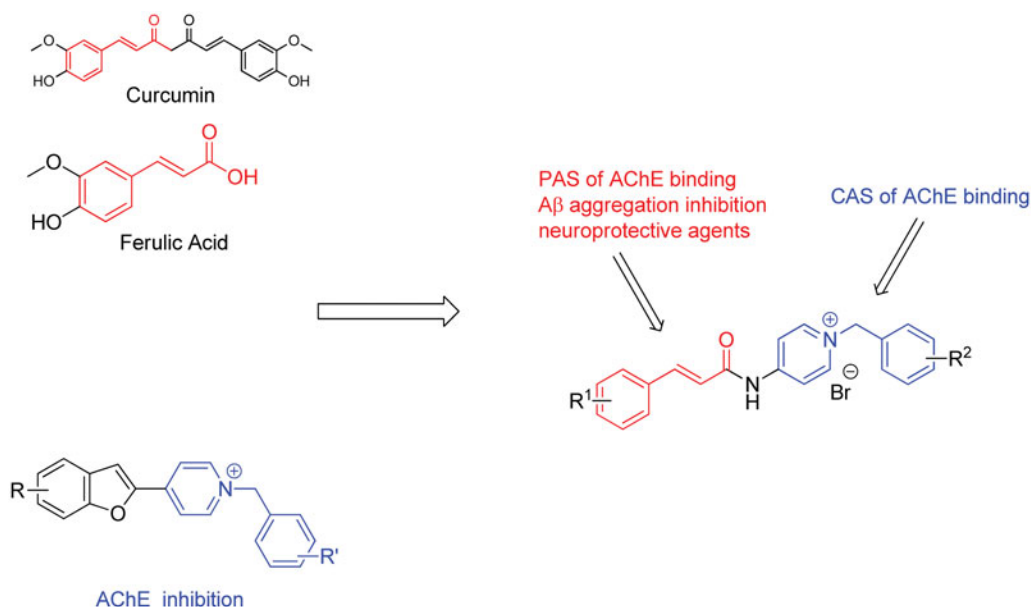


Figure 1. Drug design strategy for multi-target-directed ligands.

Therefore, ChEIs with multiple effects, such as A β disaggregation, neuroprotection and oxidative load reduction may be a significant approach for AD management.

Cinnamic acid derivatives are naturally occurring compounds that possess various pharmacological properties for diverse neurological disorders²³. Ferulic acid (FA) and curcumin (Cur) are representative bioactive compounds, and they can prevent A β fibril aggregation, inhibit A β -mediated toxicity, scavenge ROS and reduce inflammatory effects both *in vitro* and *in vivo*^{24–29}. Consequently, cinnamic acid could serve as a beneficial fragment in the designed MTDL, such as tacrine-FA hybrids, FA-memoguin hybrids, FA-carbazole hybrids, donepezil-FA hybrids, cinnamic-*N*-benzylpiperidine hybrids^{30–34}.

In the search for new cinnamic acid-based derivatives as anti-AD, we have focused on the structure of benzylpyridinium salts (Figure 1), which may represent a privileged scaffold that can be used to develop new AChE inhibitors^{35–37}. Docking studies have shown that the *N*-benzyl pyridinium moiety interacts with the CAS of AChE, and the heterocyclic moiety interacts with the PAS of AChE forming stacking interactions. Proceeding with our researches on natural products with probable use as anti-AD^{38–40}, we reasonably combined the cinnamic acid with benzyl-pyridinium to achieve new hybrids that are anticipated to be dual-acting AChE. In this study, all designed compounds were synthesised and evaluated for their biological activities, including their anti-aggregation activity towards A β , ChE inhibition, antioxidant activity, metal chelating properties, neuroprotective effects against A β -induced PC12 cell injury and the ability to cross the blood–brain barrier (BBB). Moreover, kinetic and molecular modelling studies were performed to further explore their mechanism of interaction with AChE and A β .

Materials and methods

Materials

All chemicals (reagent grade) used were purchased from Sino Pharm Chemical Reagent Co., Ltd. (Shanghai, China). Reaction progress was monitored using analytical thin layer chromatography (TLC) on pre-coated silica gel GF254 (Qingdao Haiyang Chemical Plant, Qing-Dao, China) plates and the spots were detected under UV light (254 nm). Melting point was measured on an XT-4 micromelting point

instrument and uncorrected. IR (KBr-disc) spectra were recorded by Bruker Tensor 27 spectrometer (Billerica, MA).

¹H NMR and ¹³C NMR spectra were measured on a BRUKER AVANCE III spectrometer (Billerica, MA) at 25 °C and referenced to TMS. Chemical shifts are reported in ppm (δ) using the residual solvent line as internal standard. Splitting patterns are designed as s, singlet; d, doublet; t, triplet; m, multiplet. The purity of all compounds was confirmed to be higher than 95% through analytical HPLC performed with Agilent 1200 HPLC System (Santa Clara, CA). Mass spectra were obtained on a MS Agilent 1100 Series LC/MSD Trap mass spectrometer (ESI-MS) (Santa Clara, CA).

General procedure for the preparation of compounds 3a–b

A mixture of compound **1** (10 mmol) and DMAP (10 mmol) in 20 mL anhydrous CH₂Cl₂ was stirred at 0 °C for about 10 min and EDCI (20 mmol) was added to the mixture and stirred at room temperature for 1 h. The compound **2** (10 mmol) was added to the solution, and stirring was continued overnight. The reaction mixture was diluted with H₂O and extracted with CH₂Cl₂. The organic extracts were combined, washed with brine, and dried with anhydrous Na₂SO₄, and the solvent was evaporated *in vacuo* to give the crude product, which was purified by silica gel chromatography with CH₂Cl₂:MeOH = 15:1 as an eluent to afford corresponding target compound as a yellow solid.

***N*-(pyridin-4-yl)cinnamamide (3a)** Cinnamic acid was reacted with 4-aminopyridine following the general procedure to give the desired product **3a** with a yield of 85%. ESI/MS *m/z*: 225.1 [M + H]⁺; ¹H NMR (400 MHz, CDCl₃) δ 8.75 (s, 1H), 8.50 (dd, *J* = 4.9, 1.4 Hz, 2H), 7.79 (d, *J* = 15.5 Hz, 1H), 7.64 (dd, *J* = 4.8, 1.6 Hz, 2H), 7.49 (dd, *J* = 6.6, 3.0 Hz, 2H), 7.40–7.32 (m, 3H), 6.63 (d, *J* = 15.5 Hz, 1H).

***(E)*-3-(3,4-dimethoxyphenyl)-*N*-(pyridin-4-yl) acrylamide (3b)** *(E)*-3-(3,4-dimethoxy-phenyl) acrylic acid was reacted with 4-aminopyridine following the general procedure to give the desired product **3b** with a yield of 88%. ESI/MS *m/z*: 285.2 [M + H]⁺; ¹H NMR (400 MHz, CDCl₃) δ 8.54 (d, *J* = 5.3 Hz, 2H), 7.96 (s, 1H), 7.75 (d, *J* = 15.4 Hz, 1H), 7.62 (d, *J* = 6.0 Hz, 2H), 7.15 (dd, *J* = 8.3, 1.8 Hz,

1H), 7.06 (d, $J=1.8$ Hz, 1H), 6.90 (d, $J=8.3$ Hz, 1H), 6.47 (d, $J=15.4$ Hz, 1H), 3.95 (s, 3H), 3.89 (s, 3H).

General procedure for the preparation of compounds 5a–n

Compound **3** (10 mmol), appropriate benzyl chloride (12 mmol) and a catalytic amount of KI in dry acetonitrile (20 mL) was refluxed for 1–2 h. When the reaction was completed as indicated by TLC, the mixture was then concentrated under reduced pressure, and 20 mL of diethyl ether was added. On cooling, the precipitate was filtered and washed with diethyl ether to get the target compounds **5a–n** with high yields.

1-Benzyl-4-cinnamidopyridin-1-ium bromide (5a) Yield 91%; yellow solid; IR (KBr) ν 3091, 3028, 2963, 1685, 1637, 1515, 1496, 1203, 1161, 966, 763, 752, 725 cm^{-1} ; m.p. >250 °C; ESI/MS m/z : 315.1 $[\text{M}]^+$; ^1H NMR (400 MHz, DMSO- d_6) δ 11.90 (s, 1H), 8.98 (d, $J=6.7$ Hz, 2H), 8.25 (d, $J=6.5$ Hz, 2H), 7.79 (d, $J=15.7$ Hz, 1H), 7.75–7.65 (m, 2H), 7.55–7.37 (m, 8H), 7.05 (d, $J=15.8$ Hz, 1H), 5.74 (s, 2H). ^{13}C NMR (100 MHz, DMSO- d_6) δ 165.44, 152.24, 145.20, 145.20, 143.99, 134.68, 133.93, 130.81, 129.15, 129.15, 129.15, 129.15, 129.15, 129.15, 128.50, 128.50, 128.27, 128.27, 120.20, 115.21, 61.50.

4-Cinnamido-1-(3-methylbenzyl) pyridin-1-ium bromide (5b) Yield 90%; yellow solid; IR (KBr) ν 3074, 3023, 2969, 1701, 1633, 1596, 1527, 1456, 1166, 965, 849, 743 cm^{-1} ; m.p. >250 °C; ESI/MS m/z : 329.1 $[\text{M}]^+$; ^1H NMR (400 MHz, DMSO- d_6) δ 11.80 (s, 1H), 8.94 (d, $J=6.7$ Hz, 2H), 8.22 (d, $J=6.4$ Hz, 2H), 7.80 (d, $J=15.6$ Hz, 1H), 7.70 (d, $J=4.9$ Hz, 2H), 7.49 (d, $J=5.1$ Hz, 3H), 7.33 (dd, $J=15.5$, 8.0 Hz, 2H), 7.28 (d, $J=7.6$ Hz, 1H), 7.24 (d, $J=7.5$ Hz, 1H), 6.99 (d, $J=15.7$ Hz, 1H), 5.67 (s, 2H), 2.32 (s, 3H). ^{13}C NMR (100 MHz, DMSO- d_6) δ 165.92, 152.72, 145.68, 145.68, 144.56, 139.03, 135.06, 134.42, 131.33, 131.03, 129.66, 129.66, 129.58, 129.51, 128.78, 128.78, 126.08, 120.66, 115.77, 115.77, 62.09, 21.39.

4-Cinnamido-1-(4-methylbenzyl) pyridin-1-ium bromide (5c) Yield 88%; yellow solid; IR (KBr) ν 3015, 1697, 1628, 1509, 1458, 1339, 1162, 975, 860, 761 cm^{-1} ; m.p. >250 °C; ESI/MS m/z : 329.1 $[\text{M}]^+$; ^1H NMR (400 MHz, DMSO- d_6) δ 11.84 (s, 1H), 8.93 (d, $J=6.9$ Hz, 2H), 8.23 (d, $J=6.6$ Hz, 2H), 7.79 (d, $J=15.7$ Hz, 1H), 7.70 (d, $J=4.9$ Hz, 2H), 7.49 (d, $J=5.1$ Hz, 3H), 7.40 (d, $J=7.7$ Hz, 2H), 7.26 (d, $J=7.6$ Hz, 2H), 7.01 (d, $J=15.9$ Hz, 1H), 5.67 (s, 2H), 2.31 (s, 3H). ^{13}C NMR (100 MHz, DMSO- d_6) δ 165.91, 152.68, 145.58, 145.58, 144.52, 139.18, 134.43, 132.16, 131.32, 130.18, 130.18, 129.65, 129.65, 129.08, 129.08, 128.77, 128.77, 120.68, 115.72, 115.72, 61.90, 21.22.

4-Cinnamido-1-(3-fluorobenzyl) pyridin-1-ium bromide (5d) Yield 89%; white solid; IR (KBr) ν 3075, 3018, 2966, 1701, 1632, 1589, 1526, 1448, 1146, 965, 848, 750, 676 cm^{-1} ; m.p. >250 °C; ESI/MS m/z : 333.2 $[\text{M}]^+$; ^1H NMR (400 MHz, DMSO- d_6) δ 11.84 (s, 1H), 8.96 (d, $J=6.7$ Hz, 2H), 8.23 (d, $J=6.5$ Hz, 2H), 7.80 (d, $J=15.8$ Hz, 1H), 7.70 (d, $J=4.9$ Hz, 2H), 7.54–7.45 (m, 4H), 7.42 (d, $J=9.7$ Hz, 1H), 7.34 (d, $J=7.6$ Hz, 1H), 7.28 (t, $J=8.6$ Hz, 1H), 7.00 (d, $J=15.8$ Hz, 1H), 5.74 (s, 2H). ^{13}C NMR (100 MHz, DMSO- d_6) δ 165.93, 163.72 (d, $1J_{\text{CF}}=246.44$ Hz), 152.85, 145.78, 145.78, 144.60, 137.61 (d, $3J_{\text{CF}}=7.58$ Hz), 134.41, 131.80 (d, $3J_{\text{CF}}=8.29$ Hz), 131.34, 129.66, 129.66, 128.79, 128.79, 120.64, 116.51 (d, $2J_{\text{CF}}=21.72$ Hz), 116.07 (d, $2J_{\text{CF}}=22.15$ Hz), 115.80, 61.27.

4-Cinnamido-1-(4-fluorobenzyl) pyridin-1-ium bromide (5e) Yield 95%; yellow solid; IR (KBr) ν 3083, 3022, 2969, 1626, 1509, 1462, 1338, 1158, 964, 846, 767 cm^{-1} ; m.p. >250 °C; ESI/MS m/z :

333.1 $[\text{M}]^+$; ^1H NMR (400 MHz, DMSO- d_6) δ 11.84 (s, 1H), 8.95 (d, $J=6.7$ Hz, 2H), 8.23 (d, $J=6.5$ Hz, 2H), 7.79 (d, $J=15.8$ Hz, 1H), 7.70 (d, $J=5.2$ Hz, 2H), 7.63–7.57 (m, 2H), 7.49 (d, $J=5.1$ Hz, 3H), 7.31 (t, $J=8.4$ Hz, 2H), 7.00 (d, $J=15.8$ Hz, 1H), 5.71 (s, 2H). ^{13}C NMR (100 MHz, DMSO- d_6) δ 165.92, 163.15 (d, $1J_{\text{CF}}=246.44$ Hz), 152.76, 145.61, 144.56, 137.03, 134.42, 131.62 (d, $3J_{\text{CF}}=7.98$ Hz), 131.33, 129.65, 128.78, 120.66, 116.52 (d, $2J_{\text{CF}}=21.37$ Hz), 115.77, 61.19.

1-(3-Bromobenzyl)-4-cinnamidopyridin-1-ium bromide (5f) Yield 92%; yellow solid; IR (KBr) ν 3087, 3020, 2966, 1708, 1634, 1595, 1516, 1165, 1165, 1136, 966, 837 761, 703 cm^{-1} ; m.p. >250 °C; ESI/MS m/z : 393.0, 395.0 $[\text{M}]^+$; ^1H NMR (400 MHz, DMSO- d_6) δ 11.82 (s, 1H), 8.95 (d, $J=6.8$ Hz, 2H), 8.23 (d, $J=6.5$ Hz, 2H), 7.86–7.75 (m, 2H), 7.70 (d, $J=4.8$ Hz, 2H), 7.64 (d, $J=8.3$ Hz, 1H), 7.50 (dd, $J=12.0$, 6.4 Hz, 4H), 7.43 (t, $J=7.8$ Hz, 1H), 6.98 (d, $J=15.8$ Hz, 1H), 5.72 (s, 2H). ^{13}C NMR (100 MHz, DMSO- d_6) δ 165.93, 152.85, 145.76, 145.76, 144.62, 137.60, 134.41, 132.52, 131.91, 131.81, 131.35, 129.66, 129.66, 128.79, 128.79, 128.20, 122.70, 120.64, 115.83, 115.83, 61.14.

1-(4-Bromobenzyl)-4-cinnamidopyridin-1-ium bromide (5g) Yield 90%; yellow solid; IR (KBr) ν 3020, 1707, 1624, 1514, 1460, 1336, 1141, 972, 837, 762 cm^{-1} ; m.p. >250 °C; ESI/MS m/z : 393.0, 395.0 $[\text{M}]^+$; ^1H NMR (400 MHz, DMSO- d_6) δ 11.81 (s, 1H), 8.92 (d, $J=7.4$ Hz, 2H), 8.22 (d, $J=7.2$ Hz, 2H), 7.79 (d, $J=15.8$ Hz, 1H), 7.72–7.69 (m, 2H), 7.68–7.65 (m, 2H), 7.50–7.45 (m, 5H), 6.97 (d, $J=15.8$ Hz, 1H), 5.70 (s, 2H). ^{13}C NMR (100 MHz, DMSO- d_6) δ 165.94, 152.81, 145.73, 145.73, 144.54, 134.47, 134.43, 132.56, 132.56, 131.35, 131.35, 129.65, 129.65, 128.77, 128.77, 123.06, 120.69, 115.73, 115.73, 61.19.

(E)-1-benzyl-4-(3-(3,4-dimethoxyphenyl) acrylamido) pyridin-1-ium bromide (5h) Yield 91%; yellow solid; IR (KBr) ν 3087, 3022, 2962, 1706, 1641, 1596, 1512, 1463, 1264, 1132, 1025, 965, 746, 703 cm^{-1} ; m.p. >250 °C; ESI/MS m/z : 375.1 $[\text{M}]^+$; ^1H NMR (400 MHz, DMSO- d_6) δ 11.74 (s, 1H), 8.95 (d, $J=7.4$ Hz, 2H), 8.22 (d, $J=7.3$ Hz, 2H), 7.73 (d, $J=15.6$ Hz, 1H), 7.51–7.41 (m, 5H), 7.28 (dd, $J=6.4$, 1.9 Hz, 2H), 7.06 (d, $J=8.9$ Hz, 1H), 6.89 (d, $J=15.7$ Hz, 1H), 5.72 (s, 2H), 3.85 (s, 3H), 3.80 (s, 3H). ^{13}C NMR (100 MHz, DMSO- d_6) δ 170.92, 157.60, 156.56, 154.20, 150.40, 150.40, 149.54, 139.97, 134.41, 134.41, 134.33, 133.72, 133.72, 131.95, 128.10, 122.89, 120.34, 117.04, 115.64, 115.64, 66.73, 60.90, 60.74.

(E)-4-(3-(3,4-dimethoxyphenyl) acrylamido)-1-(3-methylbenzyl) pyridin-1-ium bromide (5i) Yield 93%; yellow solid; IR (KBr) ν 3016, 1697, 1626, 1509, 1458, 1257, 1134, 1015, 971, 840, 771, 709, 593 cm^{-1} ; m.p. >250 °C; ESI/MS m/z : 389.1 $[\text{M}]^+$; ^1H NMR (400 MHz, DMSO- d_6) δ 11.69 (s, 1H), 8.91 (d, $J=7.4$ Hz, 2H), 8.20 (d, $J=7.1$ Hz, 2H), 7.73 (d, $J=15.6$ Hz, 1H), 7.36–7.22 (m, 6H), 7.06 (d, $J=8.9$ Hz, 1H), 6.84 (d, $J=15.7$ Hz, 1H), 5.66 (s, 2H), 3.85 (s, 3H), 3.80 (s, 3H), 2.32 (s, 3H). ^{13}C NMR (100 MHz, DMSO- d_6) δ 166.17, 152.81, 151.81, 149.44, 145.59, 145.59, 144.83, 139.03, 135.07, 130.22, 129.57, 129.49, 127.18, 126.05, 123.39, 118.09, 115.59, 115.59, 112.27, 110.86, 62.04, 56.14, 55.99, 21.38.

(E)-4-(3-(3,4-dimethoxyphenyl) acrylamido)-1-(4-methylbenzyl) pyridin-1-ium bromide (5j) Yield 94%; yellow solid; IR (KBr) ν 3068, 3014, 2948, 1683, 1622, 1508, 1462, 1293, 1132, 975, 794, 594 cm^{-1} ; m.p. >250 °C; ESI/MS m/z : 389.1 $[\text{M}]^+$; ^1H NMR (400 MHz, DMSO- d_6) δ 11.40 (s, 1H), 8.65 (d, $J=6.7$ Hz, 2H), 8.52 (s, 2H), 7.74 (d, $J=15.5$ Hz, 1H), 7.48 (d, $J=15.5$ Hz, 1H), 7.31–7.27 (m, 3H), 7.22–7.17 (m, 4H), 6.83 (d, $J=8.3$ Hz, 1H), 5.65 (s, 2H), 3.95 (s, 3H), 3.90 (s, 3H), 2.35 (s, 3H). ^{13}C NMR (100 MHz, DMSO- d_6) δ 166.15, 152.77, 151.81, 149.45, 145.51, 145.51, 144.82, 139.17,

132.18, 130.18, 130.18, 129.07, 129.07, 127.02, 123.39, 118.10, 115.57, 115.57, 112.29, 110.85, 61.84, 56.16, 55.99, 21.22.

(E)-4-(3-(3,4-dimethoxyphenyl) acrylamido)-1-(3-fluorobenzyl) pyridin-1-ium bromide (5k) Yield 88%; yellow solid; IR (KBr) ν 3014, 2964, 1711, 1688, 1592, 1518, 1445, 1258, 1137, 1014, 969, 850, 752, 571 cm^{-1} ; m.p. $>250^\circ\text{C}$; ESI/MS m/z : 393.1 $[\text{M}]^+$; ^1H NMR (400 MHz, DMSO-d_6) δ 11.74 (s, 1H), 8.95 (d, $J=7.4$ Hz, 2H), 8.22 (d, $J=7.0$ Hz, 2H), 7.74 (d, $J=15.6$ Hz, 1H), 7.55–7.47 (m, 1H), 7.42 (d, $J=9.8$ Hz, 1H), 7.34 (d, $J=7.7$ Hz, 1H), 7.27 (dd, $J=14.2, 4.5$ Hz, 3H), 7.06 (d, $J=8.9$ Hz, 1H), 6.88 (d, $J=15.7$ Hz, 1H), 5.74 (s, 2H), 3.83 (d, $J=4.1$ Hz, 6H). ^{13}C NMR (100 MHz, DMSO-d_6) δ 173.89, 165.13 (d, $1J_{\text{CF}}=228.26$ Hz), 161.48, 152.96, 151.82, 149.45, 145.71, 145.71, 144.85, 137.67 (d, $3J_{\text{CF}}=8.16$ Hz), 131.79 (d, $3J_{\text{CF}}=8.27$ Hz), 127.19, 125.19, 123.38, 118.10, 116.50 (d, $2J_{\text{CF}}=21.52$ Hz), 116.06 (d, $2J_{\text{CF}}=22.38$ Hz), 115.85, 115.62, 115.62, 112.28, 110.88, 61.19, 56.14, 55.98.

(E)-4-(3-(3,4-dimethoxyphenyl) acrylamido)-1-(4-fluorobenzyl) pyridin-1-ium bromide (5l) Yield 91%; yellow solid; IR (KBr) ν 3080, 3015, 1703, 1621, 1597, 1506, 1461, 1263, 1131, 1021, 964, 844, 802, 786, 596 cm^{-1} ; m.p. $>250^\circ\text{C}$; ESI/MS m/z : 393.1 $[\text{M}]^+$; ^1H NMR (400 MHz, DMSO-d_6) δ 11.69 (s, 1H), 8.91 (d, $J=7.3$ Hz, 2H), 8.19 (d, $J=7.0$ Hz, 2H), 7.72 (d, $J=15.6$ Hz, 1H), 7.58 (dd, $J=8.7, 5.4$ Hz, 2H), 7.31 (d, $J=8.9$ Hz, 1H), 7.28 (dd, $J=4.2, 2.5$ Hz, 2H), 7.05 (d, $J=8.9$ Hz, 1H), 6.83 (d, $J=15.6$ Hz, 1H), 5.69 (s, 2H), 3.82 (d, $J=3.7$ Hz, 6H). ^{13}C NMR (100 MHz, DMSO-d_6) δ 166.17, 162.94 (d, $1J_{\text{CF}}=251.49$ Hz), 152.86, 151.82, 149.45, 145.55, 145.55, 144.82, 131.60 (d, $3J_{\text{CF}}=8.08$ Hz), 131.41, 127.19, 123.37, 118.11, 116.51 (d, $2J_{\text{CF}}=21.47$ Hz), 115.60, 112.28, 110.87, 61.13, 56.15, 55.98.

(E)-1-(3-bromobenzyl)-4-(3-(3,4-dimethoxyphenyl) acrylamido) pyridin-1-ium bromide (5m) Yield 92%; yellow solid; IR (KBr) ν 2928, 2831, 1592, 1511, 1460, 1313 1137, 990, 859, 762, 710 cm^{-1} ; m.p. $>250^\circ\text{C}$; ESI/MS m/z : 453.0, 455.0 $[\text{M}]^+$; ^1H NMR (400 MHz, DMSO-d_6) δ 11.72 (s, 1H), 8.93 (d, $J=6.9$ Hz, 2H), 8.21 (d, $J=6.5$ Hz, 2H), 7.80 (s, 1H), 7.74 (d, $J=15.6$ Hz, 1H), 7.64 (d, $J=8.0$ Hz, 1H), 7.51 (d, $J=7.8$ Hz, 1H), 7.42 (t, $J=7.9$ Hz, 1H), 7.29 (s, 2H), 7.06 (d, $J=8.5$ Hz, 1H), 6.85 (d, $J=15.6$ Hz, 1H), 5.70 (s, 2H), 3.83 (d, $J=3.8$ Hz, 6H). ^{13}C NMR (100 MHz, DMSO-d_6) δ 166.17, 152.96, 151.83, 149.45, 145.68, 144.90, 137.63, 132.51, 131.90, 131.81, 128.18, 127.17, 123.41, 122.70, 118.06, 115.68, 112.28, 110.87, 61.09, 56.15, 55.98.

(E)-1-(4-bromobenzyl)-4-(3-(3,4-dimethoxyphenyl) acrylamido) pyridin-1-ium bromide (5n) Yield 88%; yellow solid; IR (KBr) ν 3012, 2948, 1681, 1618, 1508, 1460, 1268, 1130, 975, 841, 797 cm^{-1} ; m.p. $>250^\circ\text{C}$; ESI/MS m/z : 453.0, 455.0 $[\text{M}]^+$; ^1H NMR (400 MHz, DMSO-d_6) δ 11.71 (s, 1H), 8.91 (d, $J=7.3$ Hz, 2H), 8.20 (d, $J=6.9$ Hz, 2H), 7.73 (d, $J=15.6$ Hz, 1H), 7.67 (d, $J=8.4$ Hz, 2H), 7.46 (d, $J=8.4$ Hz, 2H), 7.32–7.25 (m, 2H), 7.06 (d, $J=8.9$ Hz, 1H), 6.85 (d, $J=15.7$ Hz, 1H), 5.69 (s, 2H), 3.82 (d, $J=3.7$ Hz, 6H). ^{13}C NMR (100 MHz, DMSO-d_6) δ 166.17, 152.91, 151.83, 149.45, 145.66, 145.66, 144.87, 134.51, 132.57, 132.57, 131.32, 131.32, 127.18, 123.40, 123.05, 118.08, 115.62, 115.62, 112.28, 110.86, 61.18, 56.14, 55.98.

Biological activity

In vitro inhibition studies on AChE and BuChE

Acetylcholinesterase (E.C. 3.1.1.7) from electric eel and human erythrocytes, butyrylcholinesterase (BuChE, E.C. 3.1.1.8) from equine serum and human serum, 5, 5'-dithiobis-(2-nitrobenzoic

acid) (Ellman's reagent, DTNB), S-butrylthiocholine iodide (BTCl), acetylthiocholine iodide (ATCl) and donepezil hydrochloride were purchased from Sigma-Aldrich (St. Louis, MO). The capacity of the test compounds **5a–n** to inhibit AChE and BuChE activities was assessed by Ellman's method⁴¹. Test compound was dissolved in a minimum volume of DMSO (1%) and was diluted using the buffer solution (50 mM Tris-HCl, pH =8.0, 0.1 M NaCl, 0.02 M $\text{MgCl}_2 \cdot 6\text{H}_2\text{O}$). In 96-well plates, 160 μL of 1.5 mM DTNB, 50 μL of AChE (0.22 U/mL prepared in 50 mM Tris-HCl, pH =8.0, 0.1% w/v bovine serum albumin, BSA) or 50 μL of BuChE (0.12 U/mL prepared in 50 mM Tris-HCl, pH =8.0, 0.1% w/v BSA) were incubated with 10 μL of various concentrations of test compounds (0.001–100 μM) at 37 $^\circ\text{C}$ for 6 min followed by the addition of the substrate (30 μL) ATCl (15 mM) or BTCl (15 mM) and the absorbance was measured at different time intervals (0, 60, 120 and 180 s) at a wavelength of 405 nm. The concentration of compound producing 50% of enzyme activity inhibition (IC_{50}) was calculated by nonlinear regression analysis of the response-concentration (log) curve, using the Graph-Pad Prism program package (Graph Pad Software, San Diego, CA). Results are expressed as the mean \pm SEM of at least three different experiments performed in triplicate.

Kinetic analysis of AChE inhibition

To obtain the mechanism of action **5l**, reciprocal plots of 1/velocity versus 1/substrate were constructed at different concentrations of the substrate thiocholine iodide (0.05–0.5 mM) by using Ellman's method³⁵. Three concentrations of **5l** were selected for the studies: 30.0, 15.0 and 7.5 nM for the kinetic analysis of AChE inhibition. The plots were assessed by a weighted least-squares analysis that assumed the variance of velocity (v) to be a constant percentage of v for the entire data set. Slopes of these reciprocal plots were then plotted against the concentration of **5l** in a weighted analysis and K_i was determined as the intercept on the negative x-axis. Data analysis was performed with Graph Pad Prism 4.03 software (Graph Pad Software Inc., San Diego, CA).

Molecular modeling studies

Molecular modeling calculations and docking studies were performed using Molecular Operating Environment (MOE) software version 2008.10 (Chemical Computing Group, Montreal, Canada)⁴³. The X-ray crystallographic structures of AChE (PDB code 1EVE) and A β (1–42) (PDB code PDB 1IYT) were obtained from the Protein Data Bank. All water molecules in PDB files were removed and hydrogen atoms were subsequently added to the protein. The compound **5l** was built using the builder interface of the MOE program and energy minimized using MMFF94x force field. Then the **5l** was docked into the active site of the protein by the "Triangle Matcher" method, which generated poses by aligning the ligand triplet of atoms with the triplet of alpha spheres in cavities of tight atomic packing. The Dock scoring in MOE software was done using ASE scoring function and force field was selected as the refinement method. The best 10 poses of molecules were retained and scored. After docking, the geometry of resulting complex was studied using the MOE's pose viewer utility.

ABTS radical cation scavenging activity assay⁴⁹

2,2'-Azino-bis-2-ethylbenz-thiazoline-6-sulfonic acid (ABTS) was dissolved in purified water to a 7 mM concentration. ABTS radical cation (ABTS $^{\cdot+}$) was produced by reacting ABTS stock solution with 2.45 mM potassium persulfate (final concentration) and allowing

the mixture to stand in the dark at room temperature for at least 18 h before use. The stock solution of ABTS was serially diluted with sodium phosphate buffer (50 mM, pH 7.4) to 100 μ M. Trolox and **5a–n** at different concentrations (total volume of 50 μ L) were added to 150 μ L of 100 μ M ABTS solution, respectively. After the addition of either trolox or another antioxidant to the ABTS solution, complete mixing of reactants was achieved by bubbling three to four times using plastic pipettes. The optical absorbance of ABTS at 415 nm was measured at 6 min after addition and equilibrated at 30 °C. Each individual treatment was repeated for three times and the results of the experiments were compared.

Inhibition of A β (1–42) self-induced aggregation

Inhibition of self-induced A β (1–42) aggregation was measured using a Thioflavin T (ThT)-binding assay⁴⁷. HFIP pretreated A β (1–42) samples (Anaspec Inc., Fremont, CA) were resolubilized with a 50 mM phosphate buffer (pH 7.4) to give a 25 μ M solution. Each tested compound was firstly prepared in dimethyl sulfoxide (DMSO) at a concentration of 10 mM and 1 μ L of each was added to the well of black, opaque Corning 96-well plates such that the final solvent concentration was 10%. The final concentration of each compound was 20 μ M and was prepared in independent triplicates. The solvent control was also included. Then, 9 μ L of 25 mM A β (1–42) sample was added to each well and the samples mixed by gentle trapping. Plates were covered to minimize evaporation and incubated in dark at room temperature for 46–48 h with no agitation.

After the incubation period, 200 μ L of 5 μ M ThT in 50 mM glycine–NaOH buffer (pH 8.0) was added to each well. Fluorescence was measured on a SpectraMax M5 (Molecular Devices, Sunnyvale, CA) multi-mode plate reader with excitation and emission wavelengths at 446 nm and 490 nm, respectively. The fluorescence intensities were compared and the percent inhibition due to the presence of the inhibitor was calculated by the following formula: $100 - (IF_i/IF_o \times 100)$ where IF_i and IF_o are the fluorescence intensities obtained for A β (1–42) in the presence and in the absence of inhibitor, respectively.

Metal-chelating study

The study of metal chelation was performed in methanol at 298 K using UV–vis spectrophotometer (SHIMADZU UV-2450PC, Kyoto, Japan) with wavelength ranging from 200 to 500 nm. Due to the low solubility in PBS, the compounds were tested in methanol. The absorption spectra of compound **5I** (50 μ M, final concentration) alone or in the presence of CuSO₄ and FeSO₄ (100 μ M, final concentration) for 30 min in methanol were recorded 1 cm-quartz cells. A fixed amount of compound **5I** (50 μ M) was mixed with growing amounts of Cu²⁺ (10–80 μ M) and UV spectra were recorded. Variation of absorbance at 363 nm was used to monitor the formation of **5I**/Cu²⁺ complex^{44,45}.

Inhibition of Cu²⁺-induced A β (1–42) aggregation

For the inhibition of Cu²⁺-induced A β (1–42) aggregation experiment, the A β was diluted in 20 μ M HEPES (pH 6.6) with 150 μ M NaCl. The mixture of the peptide (10 μ L, 25 μ M, final concentration) with or without copper (10 μ L, 25 μ M, final concentration) and the test compound (10 μ L, 50 μ M, final concentration) were incubated at 37 °C for 24 h. The 20 μ L of the sample was diluted to a final volume of 200 μ L with 50 μ M glycine–NaOH buffer (pH 8.0) containing ThT (5 μ M). The detection method was the same as that of self-induced A β aggregation experiment⁴⁷.

*Cell culture and measurement of cell viability*⁵⁰

The toxicity effect of the tested compounds on the rat pheochromocytoma (PC12) cells was examined according to previously reported methods. PC 12 cells was obtained from the Cell Bank of the Chinese Academy of Sciences (Shanghai, China) and routinely grown at 37 °C in a humidified incubator with 5% CO₂ in Dulbecco's modified Eagle's medium (DMEM) supplemented with 10% bovine calf serum, 100 units per mL penicillin, and 100 units per mL of streptomycin. Cells were sub-cultured in 96-well plates at a seeding density of 5000 cells per well and allowed to adhere and grow. When cells reached the required confluence, they were placed into serum-free medium and treated with compound **5I**. Twenty-four hours later the survival of cells was determined by MTT assay. Briefly, after incubation with 20 μ L of MTT at 37 °C for 4 h, living cells containing MTT formazan crystals were solubilized in 200 μ L DMSO. The absorbance of each well was measured using a microculture plate reader with a test wavelength of 570 nm and a reference wavelength of 630 nm. Results are expressed as the mean \pm SD of three independent experiments.

PC 12 cells were grown in RPMI-1640 medium containing 10% (v/v) foetal bovine serum, 100 U penicillin/mL and 100 mg streptomycin/mL under 5% CO₂ at 37 °C. The culture media were changed every other day. After pretreatment with different concentrations of test compound (0, 6, 12.5, 25, 50 μ M) for 2 h, PC 12 cells were incubated with 25 μ M of A β (1–42) for 24 h. The cell viability was evaluated using MTT assay. Briefly, the cells were treated with 10 μ L MTT (5 mg/mL in PBS) for 4 h at 37 °C. Then, 200 μ L of DMSO was added to dissolve the dark blue formazan crystals formed in intact cells, and the absorbance at 570 nm was detected by a microplate reader. PC12 cells were cultured without test compound or A β (1–42) as control group and the results were expressed by percentage of control.

In vitro BBB permeation assay

Brain penetration of compounds was evaluated using a parallel artificial membrane permeation assay (PAMPA) in a similar manner as described by Di et al.⁵¹ Commercial drugs were purchased from Sigma (St. Louis, MO) and Alfa Aesar (Haverhill, MA). The porcine brain lipid (PBL) was obtained from Avanti Polar Lipids (Alabaster, AL). The donor microplate (PVDF membrane, pore size 0.45 μ m) and the acceptor microplate were both from Millipore (Darmstadt, Germany). The 96-well UV plate (COSTAR[®]) was from Corning Incorporated (Harrodsburg, KY). The acceptor 96-well microplate was filled with 300 μ L of PBS/EtOH (7:3), and the filter membrane was impregnated with 4 μ L of PBL in dodecane (20 mg/mL). Compounds were dissolved in DMSO at 5 mg/mL and diluted 50-fold in PBS/EtOH (7:3) to achieve a concentration of 100 mg/mL, 200 μ L of which was added to the donor wells. The acceptor filter plate was carefully placed on the donor plate to form a sandwich, which was left undisturbed for 16 h at 25 °C. After incubation, the donor plate was carefully removed and the concentration of compound in the acceptor wells was determined using an UV plate reader (Flexstation[®] 3). Every sample was analyzed at five wavelengths, in four wells, in at least three independent runs, and the results are given as the mean \pm SD. In each experiment, nine quality control standards of known BBB permeability were included to validate the analysis set.

*Ex vivo brain penetration*⁵²

Fifteen male OF1 mice, weighing 25 g were used. Animals were housed under controlled light (with a 12-h light/12-h dark cycle,

lights on at 7:00 a.m.) at 25 °C and proper humidity. Rats were given food and tap water *ad libitum*.

Donepezil hydrochloride and compound **5I** were dissolved 10% DMSO. Animals were divided into three experimental handling groups: mice administered with (i) control (10% DMSO, $n=5$); (ii) donepezil (10 $\mu\text{mol/kg}$, $n=5$); (iii) compound **5I** (10 $\mu\text{mol/kg}$, $n=5$). Groups of 15 mice were treated i.p. with each compound. The animals were sacrificed 10 min later and brains were quickly removed and frozen on dry ice. Residual AChE activity was determined as previously described by the method of Ellman et al.⁴¹ using brain homogenate preparations as a source of the enzyme: A homogenate of brain samples (10%, w/v) in 0.03 M sodium phosphate buffer (pH 7.4) was prepared. The brain homogenate in volume of 200 μL was mixed with 1% Triton X-100 and centrifuged at 3000 rpm at 4 °C for 10 min. Just before analysis of the enzymatic activity, an amount of 100 μL of homogenate was diluted 2.5 times in 0.1 M phosphate-buffered solution (pH 8.0). The reaction took place in a final volume of 300 μL of 0.1 M phosphate-buffered solution (pH 8.0) containing 100 μL of diluted homogenate and 333 μM DTNB solution. To avoid interferences between AChE and BChE activities, 100 μM ISOOMPA (specific BChE inhibitor) was present in the incubation medium. Prior to the addition of the substrate acetylthiocholine, a preincubation period of 5 min was used to eliminate the endogenous ACh present in the homogenates. The reaction was started by the addition of ATCI (450 μM) and the absorbance at 414 nm was evaluated 2 min after the substrate addition. Percent of inhibition was calculated by comparing AChE

activity in brain of the drug-treated mice with activity from untreated controls.

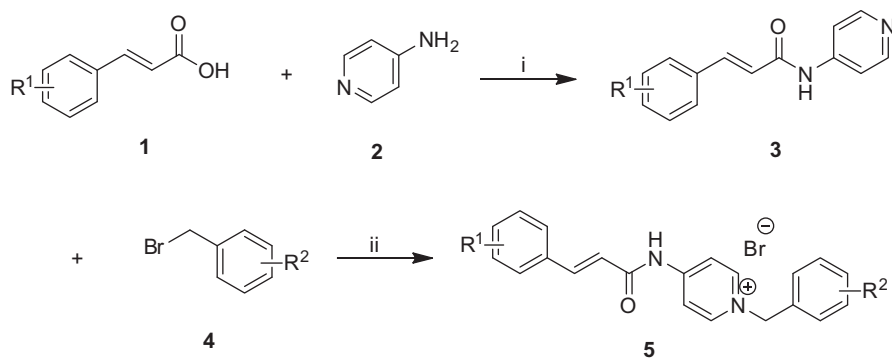
Result and discussion

Chemistry

As shown in Scheme 1, the target compounds **5a–n** were synthesized. First of all, the commercially available cinnamic acid derivatives **1** were activated with 4-dimethylaminopyridine (DMAP) and 1-(3-dimethylaminopropyl)-3-ethylcarbodiimide hydrochloride (EDCI) at 0 °C in dichloromethane solutions, and subsequently condensation with compound **2** at room temperature overnight afforded the intermediates **3**. Finally, the benzyl pyridinium bromide salts **5** were efficiently obtained by refluxing proper benzyl bromides **4** with the intermediates **3** in dry acetonitrile.

In vitro cholinesterase inhibitory activity and preliminary SAR studies

The activities of compounds **5a–n** and the relative compound cinnamic acid against AChE (from electric eel) and BuChE (from equine serum) were examined using the spectrophotometric method of Ellman et al.⁴¹ Donepezil was used as a standard compound for comparison. From Table 1, the novel cinnamic acid derivatives showed high activity towards AChE with IC_{50} values in the nanomolar range, and high selectivity for AChE over BuChE,



Scheme 1. Synthesis of cinnamic acid derivatives **5a–n**. Reagents and conditions: (i) DMAP/EDCI, CH_2Cl_2 , rt., 12 h; (ii) CH_3CN , reflux, 1–3 h.

Table 1. Inhibition of ChEs activity and selectivity index of compounds **5a–n**.

Compound	R^1	R^2	IC_{50}^a		Selectivity index (SI) ^b
			eeAChE (nM)	eqBuChE (μM)	
5a	–	–	54.1 \pm 8.2	6.3 \pm 0.6	116.5
5b	–	3- CH_3	102.6 \pm 9.6	8.1 \pm 1.3	78.9
5c	–	4- CH_3	1263.8 \pm 1.2	25.0 \pm 0.7	19.8
5d	–	3-F	93.5 \pm 7.7	7.4 \pm 0.5	79.1
5e	–	4-F	90.8 \pm 9.2	10.0 \pm 0.4	110.1
5f	–	3-Br	153.6 \pm 2.6	2.5 \pm 0.3	16.3
5g	–	4-Br	1450.5 \pm 4.3	2.1 \pm 0.8	1.5
5h	3,4-di- OCH_3	–	135.2 \pm 4.8	4.5 \pm 0.7	33.3
5i	3,4-di- OCH_3	3- CH_3	51.4 \pm 18	2.7 \pm 0.8	52.3
5j	3,4-di- OCH_3	4- CH_3	90.7 \pm 3.2	3.8 \pm 0.9	41.9
5k	3,4-di- OCH_3	3-F	20.6 \pm 1.0	3.1 \pm 0.5	150.5
5l	3,4-di- OCH_3	4-F	12.1 \pm 1.8	2.6 \pm 1.6	214.9
5m	3,4-di- OCH_3	3-Br	92.6 \pm 9.0	2.5 \pm 0.6	27.0
5n	3,4-di- OCH_3	4-Br	50.3 \pm 8.3	1.9 \pm 0.5	37.8
Cinnamic acid	–	–	>100 000	>100	–
Donepezil	–	–	40.2 \pm 3.6	4.5 \pm 0.2	112.5

^a IC_{50} : 50% inhibitory concentration (means \pm SD of three experiments).

^bSelectivity Index = IC_{50} (eqBuChE)/ IC_{50} (eeAChE).

indicating that these derivatives are selective AChE inhibitors. Among the cinnamic acid derivatives, compound **5l** ($IC_{50}=12.1$ nM) showed the most potent inhibitory activity against AChE, which was 3.3-fold higher than that of donepezil ($IC_{50}=40.2$ nM). Moreover, compound **5l** exhibited the highest selectivity level towards AChE over BuChE ($SI=214.9$). By contrast, compound **5n** exhibited the highest inhibitory activity against BuChE ($IC_{50}=1.9$ μ M), resulting 2.3-times more potent than that of donepezil ($IC_{50}=4.5$ μ M). However, the AChE inhibitory activity of cinnamic acid was remarkably low ($IC_{50}>100$ μ M), suggesting that the *N*-benzyl pyridinium moiety is unavoidably required for higher activity. The AChE inhibition by benzyl pyridinium bromide was assayed to be in the micromolar range⁴⁰, which was lower than that of novel cinnamic acid derivatives. This finding suggests that the cinnamic acid skeleton was also essential for AChE activity.

To improve the inhibitory activity of the compounds against ChEs, we introduced substituents with different sizes and electronic properties on the benzene ring of cinnamic acid and on the benzyl group of the *N*-benzyl pyridinium moiety were varied. The IC_{50} value of compounds **5a–n** indicated that the presence of methoxy groups at the positions 3 and 4 of the *N*-benzyl pyridinium moiety increased the ChE activity. For example, the ChE inhibitory activity of compounds **5i–n** was higher than that of compounds **5b–g**. Moreover, AChE inhibition was also affected by the substituents on the benzyl group. Compared with compound **5a**, the introduction of methyl, fluorine and bromine on the meta-, para-position reduced AChE inhibitory activity (compounds **5b–g**). For example, compound **5a** ($IC_{50}=54.1$ nM for AChE) was more potent than compound **5g** ($IC_{50}=1450.5$ nM for AChE) possessing 4-Br on the benzyl group. By contrast, compared with compound **5h**, compounds **5i–n** with different substituents on the benzyl group showed an increased AChE inhibitory activity. For example, compound **5l** bearing 4-F on the benzyl group exhibited more potent AChE inhibition (11-fold) than did compound **5h**. Similar to compound **5a–n** for BuChE inhibition, compounds **5f** ($IC_{50}=2.5$ μ M), **5g** ($IC_{50}=2.1$ μ M), **5l** ($IC_{50}=2.5$ μ M) and **5m** ($IC_{50}=1.9$ μ M) that were characterized by a Br substituent showed more potent inhibition. Therefore, we can rationally deduce that the size of a substituent more crucially affects BuChE inhibition than its electronic properties.

Finally compounds **5i–n** were selected for evaluation on human AChE. As listed in Table 2, all tested compounds presented IC_{50} values in the nanomolar range and were slightly more potent inhibitors for hAChE than for eeAChE. The SARs for hAChE were similar to those drawn for eeAChE inhibition (Table 1). Compound **5l** ($IC_{50}=8.6$ nM for hAChE) displayed the highest inhibition, which was fourfold higher than that of standard donepezil ($IC_{50}=33.5$ nM).

Table 2. Inhibition of ChEs activity and selectivity index of compounds **5i–n**.

Compounds	IC_{50}^a		Selectivity index ^b
	hAChE (nM)	hBuChE (μ M)	
5i	43.7 \pm 0.5	4.9 \pm 0.7	112.1
5j	96.5 \pm 2.8	5.6 \pm 1.9	58.0
5k	19.2 \pm 1.6	4.8 \pm 0.5	250.0
5l	8.6 \pm 0.9	4.4 \pm 1.2	511.6
5m	79.4 \pm 1.5	2.1 \pm 0.6	26.5
5n	51.1 \pm 4.8	1.9 \pm 0.5	37.2
Donepezil	33.5 \pm 3.8	7.6 \pm 1.9	226.9

^a IC_{50} : 50% inhibitory concentration (means \pm SD of three experiments).

^bSelectivity Index = IC_{50} (hBuChE)/ IC_{50} (hAChE).

Kinetic study of AChE inhibition

To explore the AChE inhibitory mechanism of action of the cinnamic acid derivatives, the most potent inhibitor, compound **5l**, was selected for a kinetic study using Lineweaver–Burk plots³⁹. Graphical analysis (Figure 2) revealed both increasing slopes and increasing intercepts with increasing inhibitor concentration. According to this pattern, compound **5l** is a mixed-type inhibitor for AChE and might be able to bind to the CAS and the PAS of AChE.

Molecular modeling study of AChE inhibition

To further study the dual-site mode of compound **5l** for AChE, a molecular docking study was performed using the software package MOE 2008.10^{42,43}. The X-ray crystal structure of the TcAChE complex with donepezil (hAChE, PDB code 1EVE) was applied to establish the starting model of AChE. As shown in Figure 3, the *N*-benzyl pyridinium moiety of compound **5l** was bound to the CAS of AChE, via aromatic π – π stacking interactions with the phenyl ring from Trp 84 with the ring-to-ring distance of 3.88 Å and the pyridine ring from Phe 330 with the ring-to-ring distance of 3.49 Å. Moreover, the charged nitrogen of the pyridine ring bound to the CAS was via a cation– π interaction with Trp 84 and Phe 330. The cinnamic acid moiety occupied the PAS formed by Trp 279 and Gln 74. All these results obviously indicated that compound **5l** could simultaneously bind to the PAS and CAS of AChE.

Metal-chelating properties of compound 5l

The chelating ability of compound **5l** with biometals such as Cu^{2+} and Fe^{2+} was studied using UV–vis spectroscopy (Figure 4)^{44,45}. As shown in the UV–vis spectrum (Figure 4(A)), compound **5l** without metal ions showed the absorption maximum at 216 nm and a shoulder at 353 nm. Upon the addition of $CuSO_4$, a bathochromic shift in the maximum absorption from 216 nm to 224 nm and in the shoulder from 353 nm to 363 nm occurred, suggesting the formation of the **5l**– Cu^{2+} complex. When $FeSO_4$ was added, a red shift in the maximum absorption from 216 nm to 226 nm occurred, suggesting that compound **5l** coordinates with Fe^{2+} . The complexation ability of compound **5l** might be ascribed to the dimethoxy group on the cinnamic acid moiety and to the amide moiety of the compound^{46,33}.

To determine the stoichiometry of the **5l**– Cu^{2+} complex, the molar ratio method was used, for which solutions of compound **5l** with accumulative amounts of $CuSO_4$ were prepared. The UV spectra (Figure 4(B)) showed that the absorbance at 363 nm, related to

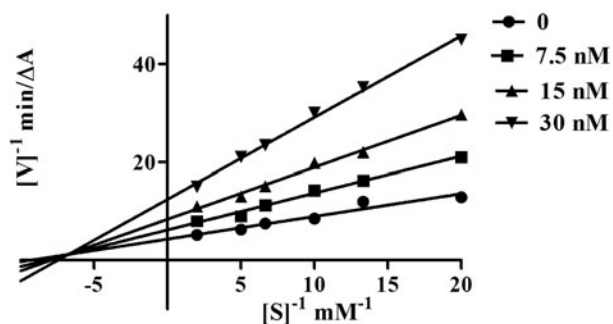


Figure 2. Kinetic study on the mechanism of EeAChE inhibition by compound **5l**. Overlaid Lineweaver–Burk reciprocal plots of AChE initial velocity at increasing substrate concentration (0.05–0.50 mM) in the absence of inhibitor and in the presence of compound **5l** are shown. Lines were derived from a weighted least-squares analysis of the data points.

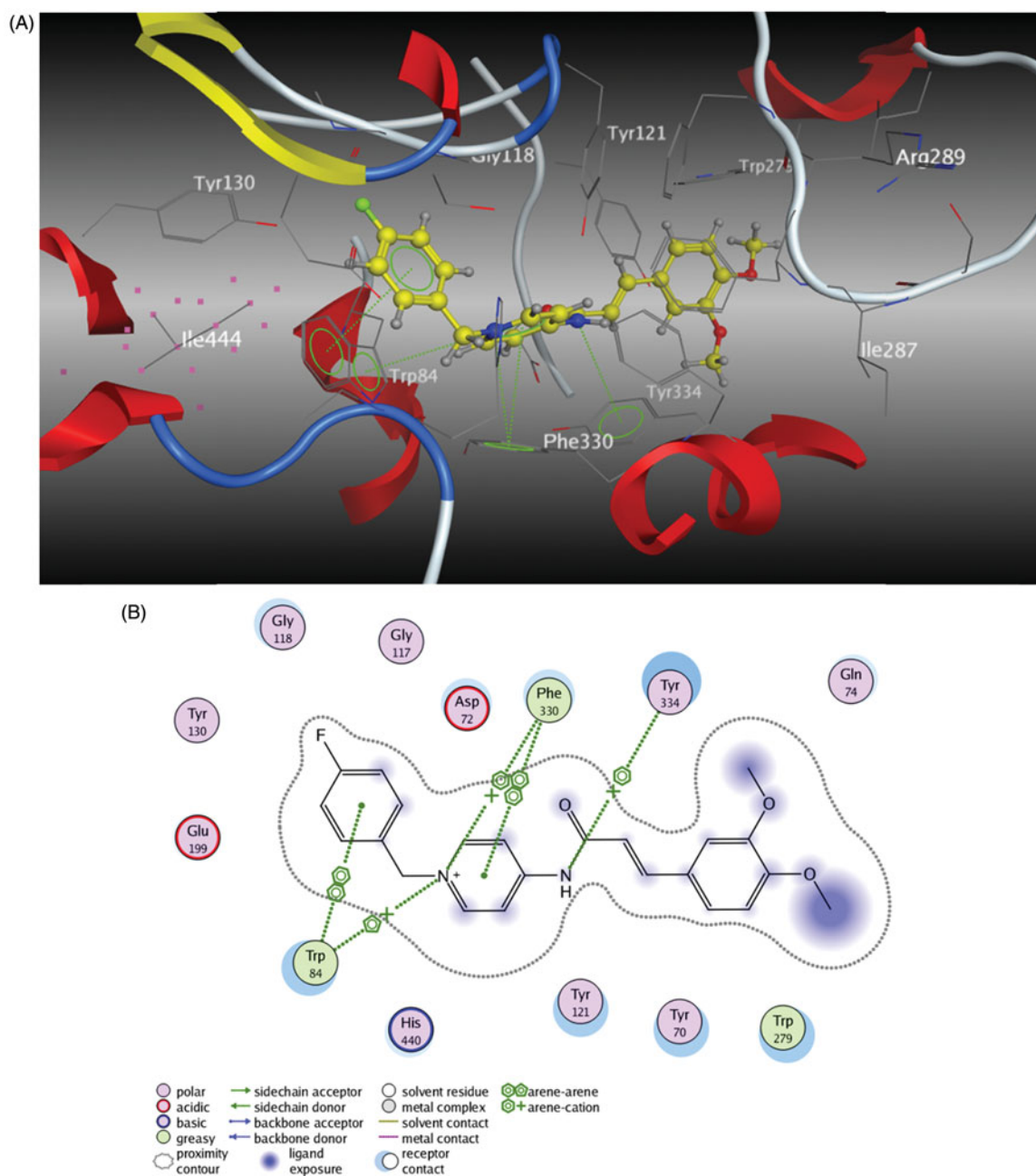


Figure 3. (A) 3D docking model of compound **5I** with TcAChE. Atom colors: yellow – carbon atoms of **5I**, gray – carbon atoms of residues of TcAChE, dark blue – nitrogen atoms, red – oxygen atoms. The dashed lines represent the interactions between the protein and the ligand. (B) 2D schematic diagram of docking model of compound **5I** with TcAChE. The figure was prepared using the ligand interactions application in MOE.

the formation of the Cu–**5I** complex, initially increased at increasing concentrations of CuCl₂ and then plateaued, and the two straight lines intersected at a mole fraction of 1.02. Thus a 1:1 stoichiometry was hypothesised for the **5I**–Cu²⁺ complex.

Inhibition of self-induced and Cu²⁺-induced Aβ (1–42) self-induced aggregation

All compounds tested for ChEs inhibition were also evaluated by a ThT-based fluorometric assay for their ability to inhibit self-induced Aβ (1–42) aggregation⁴⁷. Curcumin was used as a reference, because of its known inhibitory activity against Aβ (1–42) self-aggregation. The results are gathered in Table 3. Compounds **5a–n** exhibited good potencies (46.3–65.6% at 20 μM) compared with Cur (54.6% at 20 μM). Notably, compounds **5k**, **5l** and **5n**

(65.6%, 64.7% and 66.3%, respectively, at 20 μM) showed the highest potency. Interestingly, compounds **5h–n** with the dimethoxy group on the cinnamic acid moiety exhibited high inhibition against self-induced Aβ (1–42) aggregation with inhibition ranging from 53.9 to 66.3% at 20 μM. For example, compound **5l** (64.7% at 20 μM) was more potent than that of compound **5e** (52.8% at 20 μM). This finding led to the hypothesis that the dimethoxy group might favour Aβ aggregation inhibition. However, substituents on the benzyl group (see compounds **5i–n**) did not seem to play a role in the inhibition of Aβ (1–42) self-aggregation.

As compound **5l** showed good inhibitory activity against Aβ (1–42) self-aggregation and favourable chelating properties, its ability to inhibit Cu²⁺-induced Aβ (1–42) aggregation was investigated by a ThT-binding assay⁴⁸. Cloquinol was employed as a reference compound. As shown in Figure 5, the fluorescence of Aβ

treated with Cu^{2+} is 160.3% that of $\text{A}\beta$ alone, which points out that Cu^{2+} hastens $\text{A}\beta$ aggregation. In comparison, the fluorescence of $\text{A}\beta$ treated with Cu^{2+} and the tested compound decreased dramatically (**5l**, 68.6% inhibition of Cu^{2+} -induced $\text{A}\beta$ aggregation;

CQ, 60.2% inhibition). These results indicated that our compound could inhibit Cu^{2+} -induced $\text{A}\beta$ aggregation by effectively chelating Cu^{2+} .

Docking study of compound **5l** with $\text{A}\beta$ (1–42) peptide

To further study the interaction mode with compound **5l** for $\text{A}\beta$ (1–42), a molecular docking study was performed using the software package MOE 2008.10⁴³. The X-ray crystal structure of the protein $\text{A}\beta$ structure (PDB 1IYT) from the Protein Data Bank was used. As revealed in Figure 6, the benzene ring of cinnamic acid interacted with the His 6 via a π - π stacking interaction. A hydrogen bond interaction was also observed between the acid amides group of compound **5l** and Glu 3. These results indicated that the π - π stacking and the hydrogen bond interactions played crucial roles in the stability of the **5l**/ $\text{A}\beta$ (1–42) complex.

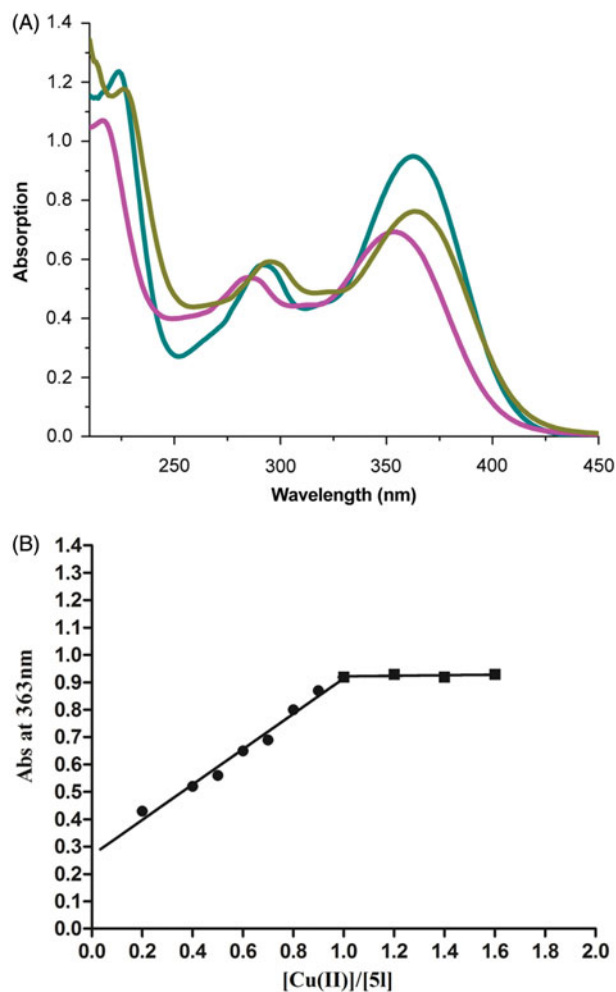


Figure 4. (A) UV absorbance spectrum of **5l** (50 μM) alone (red) or in the presence of 100 μM CuSO_4 (green) and 100 μM FeSO_4 (yellow) in MeOH. (B) Determination of the stoichiometry of complex **5l**- Cu^{2+} by molar ratio method.

Inhibition experiment

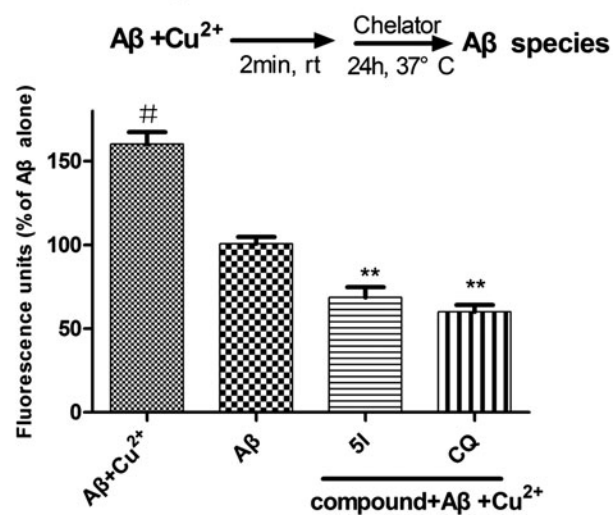


Figure 5. Inhibition of Cu^{2+} -induced $\text{A}\beta$ (1–42) aggregation by compound **5l** comparing with that of clioquinol (CQ) ($[\text{A}\beta] = 25 \mu\text{M}$, $[\text{5l}] = 50 \mu\text{M}$, $[\text{CQ}] = 50 \mu\text{M}$, $[\text{Cu}^{2+}] = 25 \mu\text{M}$, 37°C, 24 h). Values are reported as the mean \pm SD of three independent experiments. # $p < .05$, ** $p < .01$.

Table 3. Inhibition of $\text{A}\beta$ (1–42) self-induced aggregation and ABTS radical by target compounds.

Compound	R ¹	R ²	$\text{A}\beta$ (1–42) aggregation inhibition (%) ^a	ABTS assay (trolox equiv) ^b
5a	–	–	46.3 \pm 1.6	N ^c
5b	–	3-CH ₃	48.5 \pm 1.8	N
5c	–	4-CH ₃	55.1 \pm 1.5	N
5d	–	3-F	53.6 \pm 2.3	N
5e	–	4-F	52.8 \pm 1.8	N
5f	–	3-Br	48.8 \pm 2.1	N
5g	–	4-Br	57.2 \pm 1.1	N
5h	3,4-di-OCH ₃	–	55.7 \pm 3.2	N
5i	3,4-di-OCH ₃	3-CH ₃	53.9 \pm 0.9	N
5j	3,4-di-OCH ₃	4-CH ₃	63.4 \pm 2.8	N
5k	3,4-di-OCH ₃	3-F	65.6 \pm 2.3	N
5l	3,4-di-OCH ₃	4-F	64.7 \pm 1.6	N
5m	3,4-di-OCH ₃	3-Br	62.8 \pm 1.4	N
5n	3,4-di-OCH ₃	4-Br	66.3 \pm 2.9	N
Curcumin	–	–	54.6 \pm 2.6	1.65

^aInhibition of $\text{A}\beta$ (1–42) self-induced aggregation, the thioflavin-T fluorescence method was used, the mean \pm SD of at least three independent experiments and the measurements were carried out in the presence of 20 μM compounds.

^bData are expressed as (mmol trolox)/(mmol tested compound).

^cN means <0.05 .

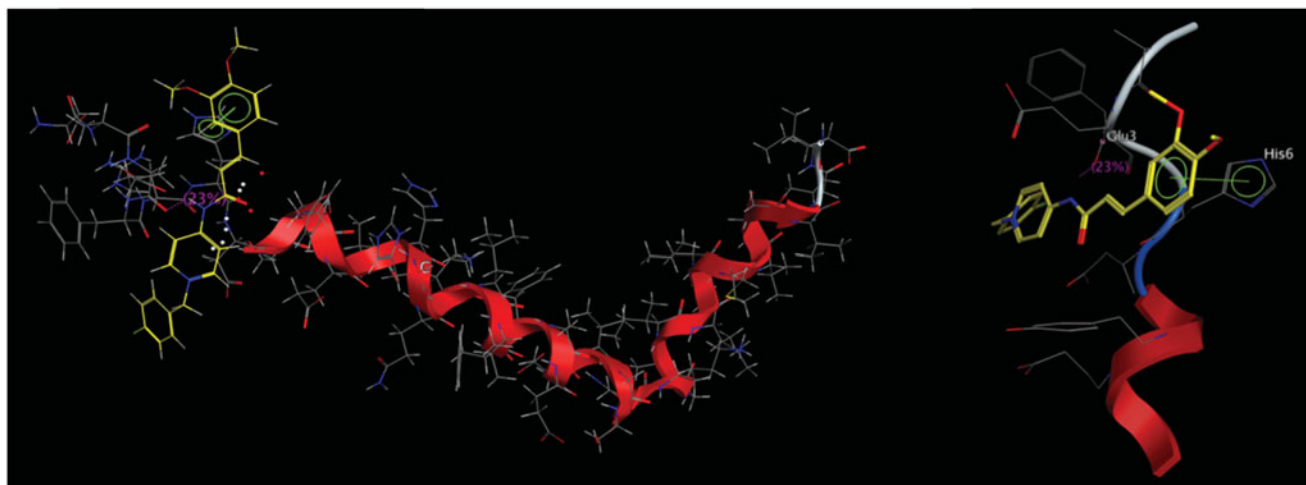


Figure 6. Docking study of compound **5I** with A β (1–42) generated with MOE. Atom colors: yellow – carbon atoms of **5I**, gray – carbon atoms of residues of A β (1–42), dark blue – nitrogen atoms, red – oxygen atoms. The dashed lines represent the interactions between the protein and the ligand.

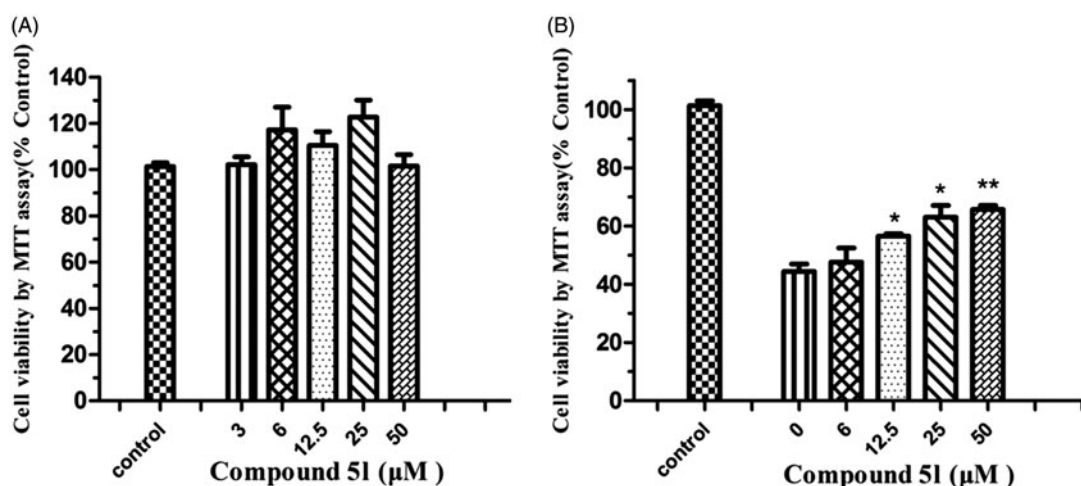


Figure 7. (A) Effects of compound **5I** on cell viability in PC12 cells. The cell viability was determined by the MTT assay after 24 h of incubation with various concentrations. The results were expressed as a percentage of control cells. Values are reported as the mean \pm SD of three independent experiments. (B) Neuroprotection against A β (1–42) toxicity. Compound **5I** was tested for neuroprotective activity against A β (1–42) toxicity in PC12 cells. Data represent the mean SD of three observations. * $p < .05$ and ** $p < .01$ compared to the A β (1–42)-treated control group.

Evaluation of compounds for antioxidant activity

The target compounds were evaluated for their antioxidant efficacy by using ABTS (ferric reducing antioxidant power) assays⁴⁹. Compared with Cur, results showed that tested compounds exhibited no antioxidant ability (Table 3). This finding might be attributed to the absence of the hydroxy group of cinnamic acid moiety.

Cytotoxicity of compound **5I** in PC12 cells and neuroprotection against A β (1–42)-induced toxicity

On the basis of the aforementioned screening results, the potential toxicity effect of compound **5I** in PC12 cells was studied⁵⁰. After incubating the cells with compound **5I** for 24 h, the cell viability was determined by the 3-(4,5-dimethylthiazol-2-yl)-2,5-diphenyltetrazolium (MTT) assay. As shown in Figure 7(A), the result revealed that compound **5I** at 3–50 μ M did not significantly affect cell viability, indicating that compound **5I** was nontoxic to neuroblastoma PC12 cells.

In the pathology of AD, A β -induced neuronal cell death is a serious event. To evaluate the neuroprotective effects of

compound **5I** against A β -induced neuronal death of PC12 cells, the data were recorded after the cells were exposed to increasing concentrations of compound **5I** (6, 12.5, 25 and 50 μ M) for 24 h. As can be seen in Figure 7(B), treatment of cells with A β (1–42) (25 μ M) to the growth medium markedly reduced cell viability to 44.2% compared with the untreated cells (control). Compound **5I** exhibited neuroprotective effects at concentrations ranging from 6 to 50 μ M (6 μ M: $47.6 \pm 4.2\%$; 12.5 μ M: $57.5 \pm 1.4\%$; 25 μ M: $63.2 \pm 3.5\%$; 50 μ M: $66.6 \pm 2.5\%$). These observations further showed that novel cinnamic acid derivatives bearing the *N*-benzyl pyridinium moiety can inhibit A β (1–42) self-aggregation for the treatment of AD.

In vitro BBB permeation assay

For successful central nervous system (CNS) drugs, the first requirement is crossing the BBB to reach brain. The potential ability of these compounds to penetrate into the brain was evaluated using a PAMPA as described by Di et al.⁵¹ Assay validation was completed by comparing the experimental permeabilities of nine commercial drugs with previously reported values (Table 4)⁵¹. A plot of the experimental data versus bibliographic values gave a

Table 4. Permeability ($P_e \times 10^{-6} \text{ cm s}^{-1}$) in the PAMPA-BBB assay for nine commercial drugs, used in the experiment validation.

Commercial drugs	Bibl ^a	PBS:EtOH (70:30) ^b
Testosterone	17	16.44
Verapamil	16	16.88
beta-Estradiol	12	11.93
Progesterone	9.3	5.34
Corticosterone	5.1	4.06
Piroxicam	2.5	1.42
Hydrocortisone	1.9	1.86
Ofloxacin	0.8	0.47
Dopamine	0.2	0.17

^aTaken from Ref.⁴⁹^bData are the mean \pm SD of three independent experiments.

good linear correlation, $P_e(\text{exp.}) = 1.06 P_e(\text{bibl.}) - 1.69$ ($R^2 = .94$). From this equation and taking into account the limit established by Di et al. for blood–brain barrier permeation, we classified the compounds as follows:

- “CNS +” (high BBB permeation predicted): $P_e (10^{-6} \text{ cm s}^{-1}) > 2.55$.
- “CNS –” (low BBB permeation predicted): $P_e (10^{-6} \text{ cm s}^{-1}) < 0.43$.
- “CNS +/-” (BBB permeation uncertain): $P_e (10^{-6} \text{ cm s}^{-1})$ from 2.55 to 0.43.

Compound **5I** with good activities against A β (1–42) aggregation and AChE was selected. The P_e value of compound **5I** was 2.89 ± 0.37 (CNS+). It indicated that compound **5I** might be able to penetrate the BBB.

Ex vivo brain penetration study

To confirm the brain permeability of compound **5I** predicted by the PAMPA, the AChE inhibitory activity was subjected to an *ex vivo* measurement after intraperitoneal (i.p.) injection of $10 \mu\text{mol/kg}$ of compound **5I** and donepezil into mice⁵². The mice were sacrificed 10 min after drug administration, and the inhibition (%) of brain AChE activity versus untreated controls was determined. Compared to control, mouse brain AChE activity was found to be inhibited by compound **5I** ($53.9 \pm 2.9\%$) and donepezil ($46.7 \pm 3.2\%$). These results confirmed that compound **5I** can cross the BBB *in vivo*.

Conclusions

In summary, novel cinnamic acid derivatives bearing *N*-benzyl pyridinium moiety were designed, synthesised and evaluated as multifunctional cholinesterase inhibitors against AD. Among the synthesised compounds, most derivatives displayed potent AChE inhibitory activity and high selectivity for AChE over BuChE. Among them, compound **5I** exhibited dual inhibitory potency on AChE and BuChE. The kinetic characterization suggested that compound **5I** acted as a mixed-type inhibition, which was consistent with the result of the molecular modelling study. Furthermore, compound **5I** showed metal-chelating ability, significant inhibition of A β aggregation and inhibition of Cu^{2+} -induced A β aggregation, in addition to low neurotoxicity. Compound **5I** also showed a neuroprotective effect against A β (1–42) toxicity in PC12 cells and was proven to penetrate into brain by the PAMPA-BBB assay *in vitro* and *ex vivo* experiments. Above all, compound **5I** could be

deemed as a multifunctional cholinesterase inhibitor and serve as a novel lead compound for treating AD.

Disclosure statement

The authors declare no conflicts of interest.

Funding

National Natural Science Foundation of China, 10.13039/501100001809 [No.81173561, 81274200, 81403175] Youth Talent Sail Plan from Shanghai Committee of Science and Technology [No. 14YF1411300] Project from Shanghai Committee of Science and Technology [No. 13401900301]

References

- Thies W, Bleiler L. Alzheimer's disease facts and figures. *Alzheimer's Dement* 2013;9:208–45.
- Tang H, Zhao HT, Zhong SM, et al. Novel oxoisoaporphine-based inhibitors of acetyl- and butyrylcholinesterase and acetylcholinesterase-induced beta-amyloid aggregation. *Bioorg Med Chem Lett* 2012;22:2257–61.
- Laferla FM, Green KN, Oddo S. Intracellular amyloid-beta in Alzheimer's disease. *Nat Rev Neurosci* 2007;8:499–509.
- Wilkinson D, Wirth Y, Goebel C. Memantine in patients with moderate to severe Alzheimer's disease: meta-analyses using realistic definitions of response. *Dement Geriatr Cogn Disord* 2014;37:71–85.
- Xie Q, Wang H, Xia Z, et al. Bis(-)-nor-meptazinols as novel nanomolar cholinesterase inhibitors with high inhibitory potency on amyloid-beta aggregation. *J Med Chem* 2008;51:2027–36.
- Munoz-Torrero D. Acetylcholinesterase inhibitors as disease-modifying therapies for Alzheimers disease. *Curr Med Chem* 2008;15:2433–55.
- Reyes AE, Chacón MA, Dinamarca MC, et al. Acetylcholinesterase-Abeta complexes are more toxic than Abeta fibrils in rat hippocampus: effect on rat beta-amyloid aggregation, laminin expression, reactive astrocytosis, and neuronal cell loss. *Am J Pathol* 2014;164:2163–74.
- Fernández-Bachiller MI, Pérez C, Monjas L, et al. New tacrine-4-oxo-4H-chromene hybrids as multifunctional agents for the treatment of Alzheimer's disease, with cholinergic, anti-oxidant, and β -amyloid-reducing properties. *J Med Chem* 2012;55:1303–17.
- Özturan Özer E, Tan OU, Ozadali K, et al. Synthesis, molecular modeling and evaluation of novel *N'*-2-(4-benzylpiperidin-1-yl)acylhydrazones derivatives as dual inhibitors for cholinesterases and A β aggregation. *Bioorg Med Chem Lett* 2013;23:440–3.
- Hardy J, Selkoe DJ. The amyloid hypothesis of Alzheimer's disease: progress and problems on the road to therapeutics. *Science* 2002;297:353–6.
- Paul S, Planque S, Nishiyama Y. Beneficial catalytic immunity to abeta peptide. *Rejuvenat Res* 2010;13:179–87.
- Bush AI. Drug development based on the metals hypothesis of Alzheimer's disease. *J. Alzheimers Dis* 2008;15:223–40.
- Fernández-Bachiller M, Pérez C, González-Muñoz GC, et al. Novel tacrine-8-hydroxyquinoline hybrids as multifunctional agents for the treatment of Alzheimer's disease, with

- neuroprotective, cholinergic, antioxidant, and copper-complexing properties. *J Med Chem* 2010;53:4927–37.
14. Price KA, Crouch PJ, White AR. Therapeutic treatment of Alzheimer's disease using metal complexing agents. *Recent Pat CNS Drug Discov* 2007;2:180–7.
 15. Ansari MA, Scheff SW. Oxidative stress in the progression of Alzheimer disease in the frontal cortex. *J Neuropathol Exp Neurol* 2010;69:155–67.
 16. Jiang CS, Fu Y, Zhang L, et al. Synthesis and biological evaluation of novel marine-derived indole-based 1,2,4-oxadiazoles derivatives as multifunctional neuroprotective agents. *Bioorg Med Chem Lett* 2015;25:216–20.
 17. Morphy R, Rankovic Z. Designed multiple ligands. An emerging drug discovery paradigm. *J Med Chem* 2005;48:6523–43.
 18. León R, Garcia AG, Marco-Contelles J. Recent advances in the multitarget-directed ligands approach for the treatment of Alzheimer's disease. *Med Res Rev* 2013;33:139–89.
 19. Agis-Torres A, Sölhuber M, Fernandez M, et al. Multi-target-directed ligands and other therapeutic strategies in the search of a real solution for Alzheimer's disease. *Curr Neuropharmacol* 2014;12:2–36.
 20. Bukhari SN, Jantan I. Synthetic curcumin analogs as inhibitors of β -amyloid peptide aggregation: potential therapeutic and diagnostic agents for Alzheimer's disease. *Mini Rev Med Chem* 2015;15:1110–21.
 21. Bajda M, Guzior N, Ignasik M, et al. Multi-target-directed ligands in Alzheimer's disease treatment. *Curr Med Chem* 2011;18:4949–75.
 22. Chen X, Decker M. Multi-target compounds acting in the central nervous system designed from natural products. *Curr Med Chem* 2013;20:1673–85.
 23. Sezgin Z, Dincer Y. Alzheimer's disease and epigenetic diet. *Neurochem Int* 2014;78:105–16.
 24. Barone E, Calabrese V, Mancuso C. Ferulic acid and its therapeutic potential as a hormetin for age-related diseases. *Biogerontology* 2009;10:97–108.
 25. Kanski J, Aksenova M, Stoyanova A, et al. Ferulic acid antioxidant protection against hydroxyl and peroxy radical oxidation in synaptosomal and neuronal cell culture systems in vitro: structure–activity studies. *J Nutr Biochem* 2002;13:273–81.
 26. Sgarbossa A, Giacomazza D, di Carlo M. Ferulic acid: a hope for Alzheimer's disease therapy from plants. *Nutrients* 2015;7:5764–82.
 27. Maruf AA, Lip H, Wong H, et al. Protective effects of ferulic acid and related polyphenols against glyoxal- or methylglyoxal-induced cytotoxicity and oxidative stress in isolated rat hepatocytes. *Chem Biol Interact* 2015;234:96–104.
 28. Hamaguchi T, Ono K, Yamada M. Review: curcumin and Alzheimer's disease. *CNS Neurosci Ther* 2015;16:285–97.
 29. Wang Y, Yin H, Wang L, et al. Curcumin as a potential treatment for Alzheimer's disease: a study of the effects of curcumin on hippocampal expression of glial fibrillary acidic protein. *Am J Chin Med* 2013;41:59–70.
 30. Benchekroun M, Bartolini M, Egea J, et al. Novel tacrine-grafted Ugi adducts as multipotent anti-Alzheimer drugs: a synthetic renewal in tacrine-ferulic acid hybrids. *ChemMedChem* 2015;10:523–39.
 31. Pan W, Hu K, Bai P, et al. Design, synthesis and evaluation of novel ferulic acid-memquin hybrids as potential multifunctional agents for the treatment of Alzheimer's disease. *Bioorg Med Chem Lett* 2016;26:2539–43.
 32. Fang L, Chen M, Liu Z, et al. Ferulic acid-carbazole hybrid compounds: combination of cholinesterase inhibition, antioxidant and neuroprotection as multifunctional anti-Alzheimer agents. *Bioorg Med Chem* 2016;24:886–93.
 33. Xu W, Wang XB, Wang ZM, et al. Synthesis and evaluation of donepezil–ferulic acid hybrids as multi-target-directed ligands against Alzheimer's disease. *Med Chem Commun* 2016;7:990–8.
 34. Estrada M, Herrera-Arozamena C, Pérez C, et al. New cinnamic – N-benzylpiperidine and cinnamic – N,N-dibenzyl(N-methyl)amine hybrids as Alzheimer-directed multitarget drugs with antioxidant, cholinergic, neuroprotective and neurogenic properties. *Eur J Med Chem* 2016;121:376–86.
 35. Baharloo F, Moslem MH, Nadri H, et al. Benzofuran-derived benzylpyridinium bromides as potent acetylcholinesterase inhibitors. *Eur J Med Chem* 2015;93:196–201.
 36. Mostofi M, Mohammadi Ziarani G, Mahdavi M, et al. Synthesis and structure–activity relationship study of benzofuran-based chalconoids bearing benzylpyridinium moiety as potent acetylcholinesterase inhibitors. *Eur J Med Chem* 2015;103:361–9.
 37. Wang C, Wu Z, Cai H, et al. Design, synthesis, biological evaluation and docking study of 4-isochromanone hybrids bearing N-benzyl pyridinium moiety as dual binding site acetylcholinesterase inhibitors. *Bioorg Med Chem Lett* 2015;25:5212–16.
 38. Lan JS, Xie SS, Li SY, et al. Design, synthesis and evaluation of novel tacrine-(β -carboline) hybrids as multifunctional agents for the treatment of Alzheimer's disease. *Bioorg Med Chem* 2014;22:6089–104.
 39. Xie SS, Lan JS, Wang XB, et al. Multifunctional tacrine-trolox hybrids for the treatment of Alzheimer's disease with cholinergic, antioxidant, neuroprotective and hepatoprotective properties. *Eur J Med Chem* 2015;93:42–50.
 40. Xie SS, Lan JS, Wang X, et al. Design, synthesis and biological evaluation of novel donepezil-coumarin hybrids as multi-target agents for the treatment of Alzheimer's disease. *Bioorg Med Chem* 2016;24:1528–39.
 41. Ellman GL, Courtney KD, Andres V, et al. A new and rapid colorimetric determination of acetylcholinesterase activity. *Biochem Pharmacol* 1961;7:88–95.
 42. Benek O, Musilek K, Horova A, et al. Preparation, in vitro screening and molecular modelling of monoquaternary compounds related to the selective acetylcholinesterase inhibitor BW284c51. *Med Chem* 2014;11:21–9.
 43. Muzammil S, Armstrong AA, Kang LW, et al. Unique thermodynamic response of tipranavir to human immunodeficiency virus type 1 protease drug resistance mutations. *J Virol* 2007;81:5144–54.
 44. Li S-Y, Jiang N, Xie S-S, et al. Design, synthesis and evaluation of novel tacrine-rhein hybrids as multifunctional agents for the treatment of Alzheimer's disease. *Org Biomol Chem* 2014;12:801–14.
 45. Sugimoto H, Tsuchiya Y, Sugumi H, et al. Novel piperidine derivatives. Synthesis and anti-acetylcholinesterase activity of 1-benzyl-4-[2-(N-benzoylamino)ethyl]piperidine derivatives. *J Med Chem* 1990;33:1880–7.
 46. Xie SS, Wang XB, Li JY, et al. Design, synthesis and evaluation of novel tacrine-coumarin hybrids as multifunctional cholinesterase inhibitors against Alzheimer's disease. *Eur J Med Chem* 2013;64:540–53.
 47. Bartolini M, Bertucci C, Bolognesi ML, et al. Insight into the kinetic of amyloid beta (1–42) peptide self-aggregation: elucidation of inhibitors' mechanism of action. *Chembiochem* 2007;8:2152–61.

48. Lu C, Guo Y, Yan J, et al. Design, synthesis, and evaluation of multitarget-directed resveratrol derivatives for the treatment of Alzheimer's disease. *J Med Chem* 2013;56:5843–59.
49. Miller NJ, Rice-Evans CA. Factors influencing the antioxidant activity determined by the ABTS.+ radical cation assay. *Free Radic Res* 1997;26:195–9.
50. Magliaro BC, Saldanha CJ. Clozapine protects PC-12 cells from death due to oxidative stress induced by hydrogen peroxide via a cell-type specific mechanism involving inhibition of extracellular signal-regulated kinase phosphorylation. *Brain Res* 2009;1283:14–24.
51. Di L, Kerns EH, Fan K, et al High throughput artificial membrane permeability assay for blood–brain barrier. *Eur J Med Chem* 2003;38:223–32.
52. Galdeano C, Viayna E, Sola, et al. Huprine-tacrine heterodimers as anti-amyloidogenic compounds of potential interest against Alzheimer's and prion diseases. *J Med Chem* 2012;55:661–9.